Interaction between the turbulent boundary layer flow of superheated vapor and the velocity field induced by liquid vaporization

E.-R. Popescu, J.R. Dawson, L. Brandt, Catherine Colin, Sébastien Tanguy

Interaction between the turbulent boundary layer flow of superheated vapor and the velocity field induced by liquid vaporization

E.-R. Popescu *[1], J. R. Dawson[1], L. Brandt[1,2], C. Colin[3], and S. Tanguy[3]

[1]Department of Energy and Process Engineering, Norwegian University of Science and Technology, Trondheim 7491, Norway
[2]FLOW, Department of Engineering Mechanics, Royal Institute of Technology (KTH), SE-100 44 Stockholm, Sweden
[3]Institut de Mécanique des Fluides de Toulouse (IMFT), Université de Toulouse, CNRS, Toulouse, France

June 5, 2023

Abstract

We consider the heat and mass transfer in the turbulent boundary layer flow over a stationary but evaporating liquid surface via direct numerical simulations. We investigate the influence of the vaporization of a static liquid pool at its saturation temperature on a fully developed turbulent boundary layer of superheated vapor, where the vaporization mass flux is treated as a boundary condition for the wall-normal velocity. It is found that the vaporization enhances the boundary layer growth whilst the friction coefficient and the Stanton number are reduced. Turbulent production is shifted further away from the wall and increased in the logarithmic layer whereas the near-wall dissipation rate is decreased in the viscous sub-layer due to the presence of non-vanishing velocity fluctuations. Spectral analysis showed an associated increase in the cross velocity energy spectrum due to vaporisation as well as a shift of the peaks towards smaller wavelengths. A similar behaviour is observed for the wall-normal turbulent heat flux spectra. The streamwise velocity energy spectrum decreases in the viscous sub-layer and increases in the logarithmic layer.

1 Introduction

Heat and mass transfer between a liquid surface and a turbulent gas or vapor stream are of significant interest in various applications, such as processes in thermal engineering, combustion, weather forecasting or climate modeling. Aside from practical applications, these configurations are also of fundamental importance to gain a better insight into how vaporisation interacts and modifies turbulence and the underlying mechanisms at play. Due to the inherent complexity of the problem, there are very few studies on these flow configurations. As such, simplifications are needed: the one adopted here is to treat the vaporization as an inflow boundary condition for the gas flow and assume the liquid pool as static [5, 26].

Previous research on turbulence modification due to wall effects has mostly focused on how a turbulent flow responds to perturbations, some of the many examples being uniform blowing or suction at the wall [32, 14, 15, 6] or through a localised spanwise slot [18, 24, 17, 34], changes in the roughness [19, 31, 22] or problems where surface heating and cooling can be used to obtain drag reduction [13]. These studies often aimed to flow control, the ultimate objective being the reduction of the friction drag on solid surfaces immersed in a turbulent flow. It has been found that the injection decreases the friction coefficient but tends to stimulate the near wall turbulence activity by increasing the Reynolds stresses [32, 14, 6] and turbulent heat fluxes [32], most prominently in the outer region [15]. The boundary layer is thickened by blowing and thinned by suction [15, 6]. The external energy injected in the flow field through blowing leads to an increased production of

*Email address for correspondence: elena.r.popescu@ntnu.no

turbulent kinetic energy in the logarithmic layer [6] and an enhancement of the fluctuation energy in the outer region [15]. Efforts were also made to investigate configurations where the perturbation is not uniform [3, 11, 27, 1, 2]. However, these studies focused on parallel channel flow configurations, where the wall-normal injection velocity was either sinusoidally variying in the streamwise direction [27], or time-periodic [1, 2].

Fewer investigations considered the effects of blowing or suction that depend of the local thermal field. Lakehal *et al.* [20] performed a pseudospectral DNS to study the effect of condensation on turbulence in a stratified steam-water flow for variable interfacial shear velocities and liquid subcooling rates. Their analysis revealed that the interfacial waves were damped by condensation and the streamwise vortical structures on the liquid side were attenuated. A DNS with modelling of the turbulent boundary layer over an evaporating liquid film was considered by Desoutter *et al.* [5]. The liquid film surface was modelled via a boundary condition with the objective of proposing new dimensionless variables for wall functions that depend upon the temperature and the mass species fields in the presence of an evaporation blowing velocity.

Popescu *et al.* [26] conducted DNS to examine the influence of vaporization or condensation of a static liquid pool at saturation on a laminar boundary layer of superheated or subcooled vapor, showing that the normal velocity induced by the phase change significantly changes the vapor thermal field in the vicinity of the liquid/vapor interface. The authors proposed new correlations on the heat transfer at the liquid/vapor interface as a function of the phase change rate and of the dimensionless numbers defining the flow. However, in most of the applications the flow of the gas stream is turbulent, which is the subject of the present study.

In this paper, we report the results of a DNS aiming to shed some light on the influence of vaporization of a static liquid pool at its saturation temperature on a fully developed turbulent boundary layer of superheated vapor. Here, we do not simulate the liquid layer as it has been shown in [26] that the vapor stream has a negligible influence on the liquid field. The novelty of this investigation, compared with the aforementioned studies, is that the blowing velocity varies both in time and in space, depending on the local temperature fluctuations. Indeed, the normal velocity due to the vaporization is obtained from the values of the temperature and temperature gradient at the interface, assumed planar. Nevertheless we consider a two-way interaction where the interface mass flux due to vaporization alters the boundary layer, thereby changing the velocity profiles. This, in turn, affects the temperature field and its gradient near the liquid interface and thus alters the vapor injection onto the boundary layer. To avoid the additional computational cost associated with the simulation of the liquid field, the vaporization mass flux is treated as a boundary condition for the wall-normal velocity on the plane surface defining the liquid interface, with tangential velocity set to zero.

The paper is divided into two parts. Section 2 describes the numerical procedure, with an emphasis on the turbulence injection technique, which allows for the simulation of a fully developed turbulent boundary layer with heat transfer. In this section, the computation of the normal velocity generated by vaporization and imposed as a boundary condition at the wall is also described. The results obtained are presented in section 3, where the effects of the blowing velocity induced by vaporization on the turbulent boundary layer structure are studied through statistics and spectral analysis of the turbulent structures. In order to highlight the differences between the vaporization and uniform blowing on the turbulence structure, we have also conducted simulations with a constant blowing velocity and showed the results for comparison.

2 Numerical procedure

The flow configuration studied in this work consideres the interaction between the normal velocity generated by the liquid/vapor phase change and a spatial developing turbulent boundary layer with heat transfer. Through a dimensional analysis of the Navier-Stokes,

$$\frac{\partial \mathbf{u}}{\partial t} + (\mathbf{u} \cdot \nabla)\,\mathbf{u} = -\nabla p + \frac{1}{Re}\nabla^2 \mathbf{u}, \tag{1}$$

and energy equations,

$$\frac{\partial \Theta}{\partial t} + (\mathbf{u} \cdot \nabla)\,\Theta = \frac{1}{RePr}\nabla^2 \Theta, \tag{2}$$

it can be shown that the flow under investigation is described by four dimensionless numbers: the Reynolds number $Re_\theta = U_\infty \theta/\nu$, the Prandtl number $Pr = \mu C_p/\lambda$, the Jakob number $Ja = C_p \Delta T/L_v$ and the density ratio ρ_v/ρ_l, with U_∞ the upstream flow velocity, θ the momentum boundary layer thickness, ν the kinematic viscosity, μ the dynamic viscosity, C_p the specific heat at constant

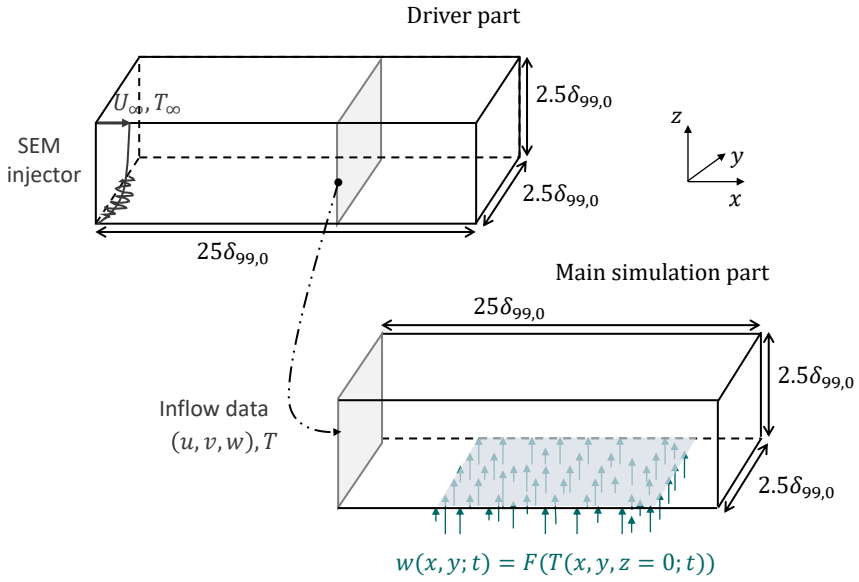

Figure 1: Schematic of the numerical configuration and coordinate system adopted.

pressure, λ the thermal conductivity, ΔT the thermal gradient, L_v the latent heat and ρ the density. The latter two numbers, Ja and ρ_v/ρ_l, characterize the phase change flow rate, $\dot{m}$.

In this study we assume equivalence between the streamwise velocity and the temperature field as reported in several studies [25, 9]. Hence, the temperature equation 2 is transformed using a reduced temperature field defined by

$$\tilde{T} = \frac{\Theta_\infty - \Theta}{\Theta_\infty - \Theta_0}, \tag{3}$$

with Θ_∞ the temperature outside the boundary layer, $\Theta_0 < \Theta_\infty$ the temperature at the wall and $\tilde{T} \in [0, 1]$. To avoid an increase of the computational cost due to the need to increase the size of the computational domain due to a thicker thermal boundary layer, ($Pr < 1$) or the need of a finer mesh when $Pr > 1$, the Prandtl number is set to $Pr = 1$, so that the thermal and momentum boundary layers have the same thickness.

The computations consist of two steps, as shown in figure 1: the driver, needed to generate inflow conditions, and the main simulation. In the driver part, a zero-pressure-gradient turbulent boundary layer flow with associated temperature field is generated using at the inlet plane the Synthetic Eddy Method (SEM) [10] for the synthetic inflow generation. Once the turbulence is well developed and recovers a realistic structure, verified through the second order statistics and energy budgets, cross-stream velocity and temperature planes are saved and stored at each time step. These are used as inflow boundary condition for the main simulation.

The computational domain is $l_x \times l_y \times l_z = (25 \times 2.5 \times 2.5)\,\delta_{99,in}$ for both simulations, with $n_x \times n_y \times n_z = 1024 \times 128 \times 128$. The boundary layer thickness, $\delta_{99,in}$, is defined by the wall-normal location at the inlet plane where the local velocity is $99\%U_\infty$. Here, we denote with x and y the streamwise and spanwise directions and with z the distance from the wall. A uniform mesh is used in the streamwise and spanwise directions while a non-uniform grid, refined close to the wall by a hyperbolic tangent function, is adopted in the wall-normal direction. The corresponding grid spacing in wall units are $\Delta x^+ = 11$, $\Delta y^+ = 8.7$ and $\Delta z^+_{min} = 1.1$, $\Delta z^+_{max} = 18$. The non-dimensionalization in wall units uses the inlet friction velocity and the kinematic viscosity, i.e. $\Delta x^+ = \Delta x u_{\tau,in}/\nu$. The non-dimensional time step $\Delta t^+ = \Delta t u^2_{\tau,in}/\nu$ is about 0.17.

For both the driver and the main part, periodic boundary conditions are imposed on the velocity and thermal fields in the spanwise direction. At the upper free stream boundary and at the outlet, outflow boundary conditions are imposed, derived accounting for the continuity condition,

$$\frac{\partial u}{\partial z} = 0, \quad \frac{\partial v}{\partial z} = 0, \quad \frac{\partial w}{\partial z} = -\left(\frac{\partial u}{\partial x} + \frac{\partial v}{\partial y}\right), \quad \text{for } z = l_z, \tag{4}$$

and

$$\frac{\partial v}{\partial x} = 0, \quad \frac{\partial w}{\partial x} = 0, \quad \frac{\partial u}{\partial x} = -\left(\frac{\partial v}{\partial y} + \frac{\partial w}{\partial z}\right), \quad \text{for } x = l_x. \tag{5}$$

For the temperature field, Neumann boundary conditions are applied, $\left(\frac{\partial T}{\partial z}\right)_{z=l_z} = 0$ and $\left(\frac{\partial T}{\partial x}\right)_{x=l_x} = 0$.

In the driver simulation, we prescribe the non-slip condition at the wall and an isothermal boundary condition for the temperature. The inflow boundary condition at the inlet plane $x = 0$, for both the velocity and the temperature fields, is prescribed according to the SEM [10, 23], described in section 2.2.

In the main simulation, the liquid/vapor phase change is treated as a boundary condition on the normal velocity w at the wall, as detailed below. Note that the vaporization happens only in the region $[6 - 18]\delta_{99,in}$, to avoid numerical artefacts related to the interaction of the wall blowing with inflow and outflow boundary conditions. Additionally, as the dynamical coupling between temperature and velocity is done only at the wall boundary condition, the temperature can still be considered a scalar field inside of the computational domain.

2.1 The phase change as a boundary condition

It has been shown [26] that when considering the laminar boundary layer flow over an overheated or subcooled static liquid, the shear from the vapor creates negligible velocity in the liquid for a low viscosity ratio and on a short length of interaction. As a consequence, and to save the computational costs associated with the resolution of the liquid phase, we model the liquid/vapor phase change as a boundary condition for the normal velocity. The latter is computed from the expression of the mass flow rate at the liquid/vapor interface Γ. Imposing continuity at the liquid/vapor interface leads to a jump condition on the velocity field,

$$[\mathbf{u}]_\Gamma = \dot{m} \left[\frac{1}{\rho}\right]_\Gamma \mathbf{n}, \tag{6}$$

where $\dot{m}$ is the mass flow rate, proportional to the interface thermal flux,

$$\dot{m} = \frac{1}{L_v} \left[\lambda \frac{\partial \Theta}{\partial z}\right]_\Gamma. \tag{7}$$

Further, assuming a plane interface between the vapor and the static liquid pool at saturation, with normal $\mathbf{n} = \mathbf{e}_z$, the velocity in the liquid is zero $\mathbf{u}_l = 0$ and the temperature equal to the saturation temperature, $\Theta_l(x, y, z) = \Theta_{sat}$. Consequently, equations (6) and (7) reduce to

$$[w]_\Gamma = \dot{m} \left(\frac{1}{\rho_v} - \frac{1}{\rho_l}\right), \quad \text{with} \quad \dot{m} = \frac{1}{L_v} \left(\lambda_v \frac{\partial \Theta}{\partial z}\Big|_{z=0}\right). \tag{8}$$

The liquid/vapor phase change is therefore imposed as an inflow boundary condition at $z = 0$, with $u = v = 0$ and $w = \dot{m}\,(1/\rho_v - 1/\rho_l)$. The mass flow rate $\dot{m}$ is obtained at each time step, using the local vapor temperature gradient at $z = 0$. As we simulate the reduced temperature field $\tilde{T}$, the mass flow rate is re-written as

$$\dot{m} = \frac{(\Theta_\infty - \Theta_0)}{L_v} \left(\lambda_v \frac{\partial \tilde{T}}{\partial z}\Big|_{z=0}\right).$$

2.2 Synthetic Eddy Method (SEM)

The SEM [10] generates a velocity signal with prescribed first- and second-order moments in a three-dimensional virtual box. The operation uses the Cholesky decomposition $A_{ij}(z)$ of a prescribed Reynolds stress tensor $R_{ij}(z)$ to assign second-order moments to a normalized stochastic signal $\widetilde{u}_j(x, y, z; t)$ superimposed on a mean velocity $U_i(z)$,

$$u_i(x, y, z; t) = U_i(z) + \sum_j A_{ij} \tilde{u}_j(x, y, z; t), \tag{9}$$

where $\tilde{u}_j(x, y, z; t)$ is a centered random sequence with unit variance and zero covariance.

The inlet plane, at $x = 0$, is defined by a finite set of points $S = \{\mathbf{x}_1, \mathbf{x}_2, ..., \mathbf{x}_s; \mathbf{x} = (0, y, z)\}$ on which the synthetic velocity fluctuations are generated. Assuming that the mean velocity U_i, the Reynolds stresses R_{ij} and a characteristic length scale of the coherent structures σ are avalaible for the set of points considered, the first step is to create a box, of volume V_B, which contains the

synthetic eddies. The dimensions of the box are chosen in such a way that all the points in S are surrounded by eddies,

$$B = \left\{ x_i^E = (x^E, y^E, z^E) \in \mathbb{R}^3 : x_{i,min}^E \leq x_i^E \leq x_{i,max}^E \right\}, \tag{10}$$

where $x_{i,min}^E = \min\left(x_i^E - \sigma(\mathbf{x}_S)\right)$ and $x_{i,max}^E = \max\left(x_i^E + \sigma(\mathbf{x}_S)\right)$.
The size of an eddy used in the generation of the synthetic inflow is defined as

$$\sigma(z) = \max\left\{ \min\left\{ \left|(k')^{3/2}/\epsilon\right|, \kappa\delta_{99,in} \right\}, \max\left(\Delta x, \Delta y, \Delta z\right) \right\},$$

where k' is the turbulent kinetic energy, ϵ is the dissipation, $\kappa = 0.41$ is the von Karman constant. The influence of thermal fluctuations on the coherent turbulent structures is not considered as $Pr = 1$ and $Pr_t = 1$.

The velocity signal generated by the N eddies is expressed by

$$\tilde{u}_i(y,z) = \frac{1}{N} \sum_{k=1}^{N} \epsilon_{i,k} f_{\sigma(\mathbf{x})}\left(\mathbf{x} - \mathbf{x}_k^E\right), \tag{11}$$

where $\mathbf{x}_k^E$ are the locations of the N eddies and $\epsilon_{i,k}$ are independent variables taken from any distribution with zero mean and unit variance. We choose $\epsilon_{i,k} \in \{-1, 1\}$ with equal probability. The velocity distribution of the eddy located at $\mathbf{x}_k^E$ is represented by the function f_σ. It is assumed that the differences in the distributions between the eddies depend only on the length scale σ,

$$f_\sigma = \sqrt{V_B \sigma^{-3}} f\left(\frac{x_k^E}{\sigma}\right) f\left(\frac{y - y_k^E}{\sigma}\right) f\left(\frac{z - z_k^E}{\sigma}\right). \tag{12}$$

The shape function f is common to all eddies, with compact support in $[-\sigma, \sigma]$ and normalization $\int_{-\sigma}^{+\sigma} f^2(x)dx = 1$. The factor $\sqrt{\sigma^{-3}}$ imposes the normalization condition.

The positions of the eddies $\mathbf{x}_k^E$ before the first time step are independent from each other and taken from a uniform distribution. At each time step, the eddies are convected through B with a characteristic velocity U_c. For more details on the different steps of the SEM implementation, the interested reader is referred to [10].

Concerning the implementation in the present study, the database pertaining a boundary layer with momentum thickness Reynolds number $Re_{\theta,in} = 1100$ by Jimenez *et al.* [12] is used to configurate the SEM, i.e. the mean velocities U_i and the Reynolds stress tensor R_{ij}. The thermal fluctuations at the inlet plane are generated with the extended SEM in [23]. As for the dynamic boundary layer, the temperature Θ imposed at the inlet plane reads

$$\Theta(0, y, z; t) = T(z) + \theta_{rms}(z)\tilde{\Theta}(y, z; t), \tag{13}$$

where the mean T and rms temperature θ_{rms} are specified at the inlet plane using the same database [12] as for the velocity inflow.

The generated eddies are convected throughout the box B using the mean of the averaged velocity at the inlet plane U_c.

2.3 Flow solver

The numerical simulations have been conducted using the open source code *CaNS* [4]. The governing fluid and thermal equations are solved using an efficient algorithm for massively-parallel simulations of incompressible turbulent flows. The method uses second-order finite-differences for spatial discretization with a staggered disposition of grid points, and a low-storage, three-step Runge-Kutta scheme for the time integration. The pressure Poisson equation is solved with the method of eigenfunction expansions, allowing to use very efficient FFT-based solvers. We refer to [4] for more details on the flow solver.

3 Results

In this section we report results of the DNS of the interaction between a turbulent boundary layer flow with heat transfer and the normal velocity induced by vaporization. In order to highlight the

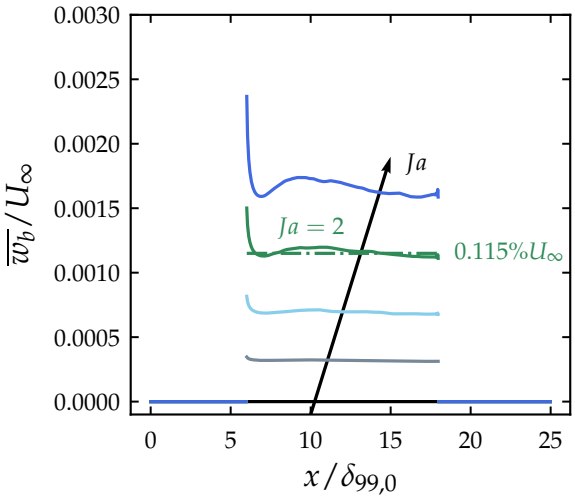

Figure 2: Streamwise profiles of the mean wall-normal velocity imposed by the vaporization boundary condition, $\overline{w_b}/U_\infty$, for different values of the Jakob number $Ja = [0, 0.4, 1, 2, 3.52]$. The profiles have been obtained after an average in time and in the spanwise direction. The constant velocity $w_b = 0.115\%U_\infty$, corresponding to the uniform blowing configuration, has also been plotted for comparison.

differences between the vaporization and uniform blowing on the turbulence structure, we have also conducted simulations with a constant blowing velocity which will also be discussed here.

To confirm that the turbulent boundary layer is well developed before applying the blowing we will compare our results with available numerical and experimental data. Additionally, we show the streamwise evolution of the integral quantities for both the auxiliary and main simulations in order to demonstrate the continuity in the spatial development of the boundary layer between the two simulations.

Statistics are collected after the flow has travelled twice through the computational domain by averaging in time and in the spanwise direction. The different quantities are sampled every fifth computational time step for about 60 units in terms of $\delta_{99,in}/u_{\tau,in}$.

The blowing velocity is computed using the thermal gradient, so it is varying in both time and space, translating the vaporization rate into a boundary condition on the normal velocity. The dimensionless number that characterizes the vaporization rate is the Jakob number, $Ja = C_p\Delta T/L_v$. Several values of Ja are considered here, $Ja = [0, 0.4, 1, 2, 3.52]$, corresponding to increasing vaporization rates. Each value of the Jakob number requires to perform a new simulation.

The profiles of the mean wall-normal velocity, imposed by the vaporization boundary condition (Eq. 8), are displayed in Figure 2. The profiles have been averaged in time and in the spanwise direction. The blowing velocity increases with the vaporization rate, quantified by the Jakob number, Ja, and vary in the streamwise direction, with a peak at the junction between unperturbed/perturbed flow at $x/\delta_{99,0} = 6$. This can be explained by the presence of higher streamwise gradients in the temperature field. Indeed, with vaporization, the temperature decreases with blowing in the region $x/\delta_{99,0} = [6, 18]$. The constant velocity $w_b = 0.115\%U_\infty$, used in the simulation with uniform blowing is also depicted to show that, in terms of blowing intensity, the uniform blowing case should be directly compared with the vaporization configuration with $Ja = 2$.

First, to visualize the flow under investigation, we display in figure 3 isosurfaces of the Q-criterion and the vorticity magnitude in one (x, z) plane, for the three cases: unperturbed flow, uniform blowing and blowing induced by vaporization at $Ja = 2$. The quantity Q represents the local balance between shear strain rate and vorticity magnitude, defining vortices as areas where the vorticity magnitude is greater than the magnitude of the rate-of-strain [8]. In order to highlight the thickening of the boundary layer, the Q criterion isosurfaces are colored with the distance to the wall. The figure reveals that the turbulence is enhanced by the blowing at the wall, both by the uniform and vaporization induced blowing. Park *et al.* [24] studied the effects of uniform blowing, introduced through a slot, on near-wall vortices and observed that the vortical structures are lifted up and become much stronger downstream of the slot. This can also be observed in the present study. However, in the case of vaporization, we can observe a high increase in the population of coherent structures both in the region where blowing is active as well as downstream of it. Additionally,

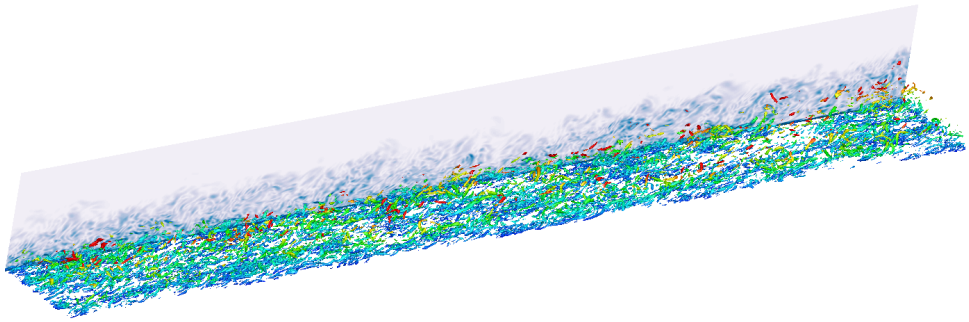

(a) Without blowing ($Ja = 0$).

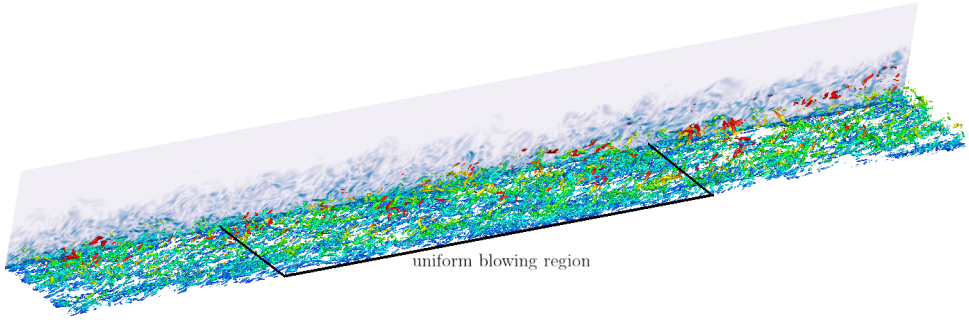

(b) Uniform blowing ($U_b = 0.11\%U_\infty$).

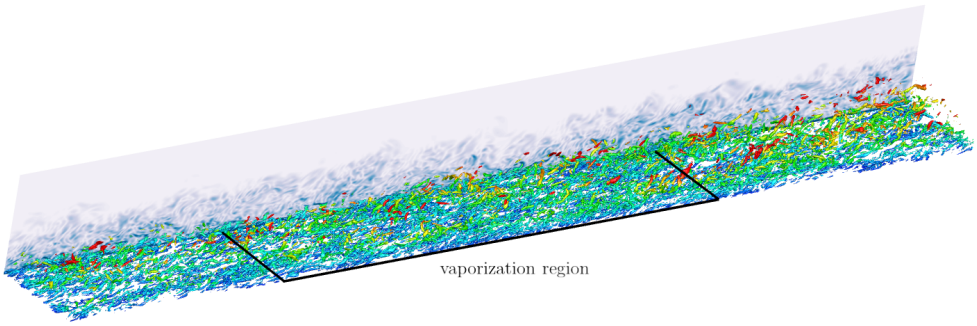

(c) With blowing ($Ja = 2$).

Figure 3: Isosurfaces of the Q-criterion, value $Q = 0.5$, colored as function of the wall-normal distance, and contours of the vorticity magnitude in a (x, z) plane. The figures highlight the influence of the blowing on the spatial development of the turbulent boundary layer flow.

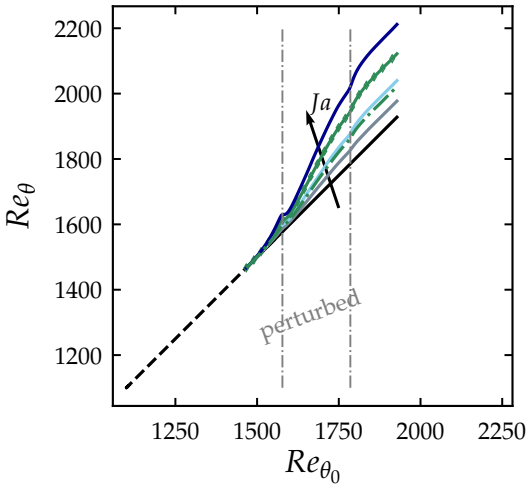

Figure 4: Streamwise evolution of the momentum thickness Reynolds number Re_θ as a function of the momentum thickness Reynolds number without blowing $Re_{\theta,0}$: (- -), the auxiliary simulation and (—) the main simulation for different values of the Jakob number $Ja = [0, 0.4, 1, 2, 3.52]$, as well as for the uniform blowing (-··-). The latter can be compared in terms of blowing intensity to the case $Ja = 2$ (-♦-). The perturbed zone where blowing occurs is indicated on the graph by the two vertical lines.

more structures are present further away of the wall, i.e. red colored structures, than in the case of uniform blowing which underlines the stronger effect induced by vaporization in comparison to uniform blowing.

3.1 Global measures

We first examine the global flow behavior and then focus on the single point velocity and temperature statistics, to conclude with the spectral analysis. Figure 4 displays the evolution of the momentum Reynolds numbers for uniform blowing and for non-uniform blowing at different values of the Jakob number, $Ja = [0, 0.4, 1, 2, 3.52]$, as a function of the momentum thickness Reynolds number $Re_{\theta,0}$ pertaining the flow without evaporation. Note that hereinafter $Re_{\theta,0}$ indicates the momentum thickness Reynolds number of the unperturbed flow. This choice allows us to compare data at the same physical downstream location. It is found that both uniform blowing and vaporization are promoting the spatial growth of the boundary layer thickness. However, when comparing uniform blowing at constant velocity $w_b = 0.115\%U_\infty$ and its corresponding vaporization case at $Ja = 2$, the latter shows a stronger influence on the increase of the boundary layer thickness. For the vaporization configurations, the growth of Re_θ increases with the value of Jakob number and it was found that, for a fixed $Re_{\theta,0}$, the dependency on the Jakob number is best approximate with a second order polynomial. Finally, we note that the bumps at the upstream and downstream edges of the blowing region are induced by the pressure gradient due to blowing, as also reported in [15].

In figure 5 we report the evolution of the friction Reynolds number, Re_τ, with the momentum thickness Reynolds number, $Re_{\theta,0}$. The friction Reynolds number quantifies the ratio of the outer to inner length scales. First, we note that both the evolution obtained for $Ja = 0$, and the one obtained from the auxiliary simulation are in agreement with the numerical results from [30]. Further, we note that the blowing decreases the friction Reynolds number: at fixed downstream location, the outer length scale δ_{99} decreases in comparison with the inner length scale ν/u_τ, more so when increasing the value of the Jakob number. This decrease can be fitted with a second order polynomial in terms of the Jakob number, as shown in the inset in figure 5. Upstream and downstream of the vaporization zone, the curves follow the same trend as the configuration $Ja = 0$. The same effect is found when the blowing is uniform. However, the decrease is weaker in comparison with the vaporization case: for a fixed $Re_{\theta,0} = 1700$, the vaporization at $Ja = 2$ decreases by 10% more the friction at the wall, i.e. $Re_\tau(Ja = 2)/Re_\tau(Ja = 0) = 0.92$ and $Re_\tau(w_b = 0.115\%U_\infty)/Re_\tau(Ja = 0) = 0.82$.

The effect of blowing on the local values of the friction coefficient C_f,

$$C_f = \frac{2\tau_w}{\rho U_\infty^2}, \tag{14}$$

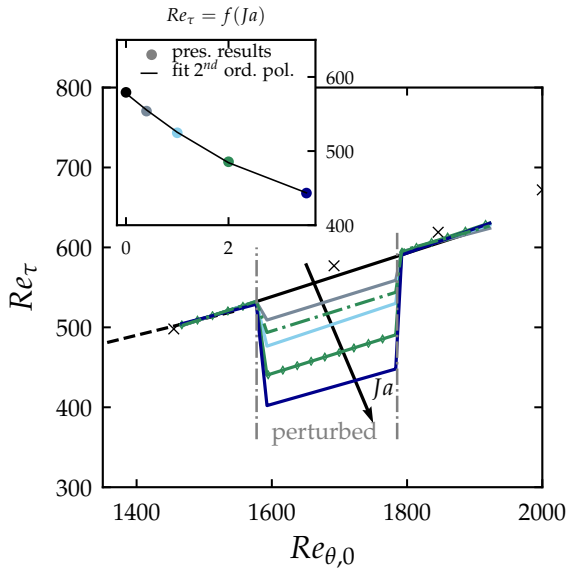

Figure 5: Streamwise evolution of the friction Reynolds number Re_τ versus the momentum thickness Reynolds number without blowing $Re_{\theta,0}$: (×), [30], (- -), the auxiliary simulation and (—) the main simulation for different values of the Jakob number $Ja = [0, 0.4, 1, 2, 3.52]$, as well as for the uniform blowing (-·-). The latter can be compared in terms of blowing intensity to the case $Ja = 2$ (-♦-). The perturbed zone where blowing occurs is equally indicated on the graph. The inset figure displays Re_τ versus the Jakob number at a fixed $Re_{\theta,0} = 1750$. The points can be fitted with a second order polynomial, $5.68Ja^2 - 58.1Ja + 577.8$.

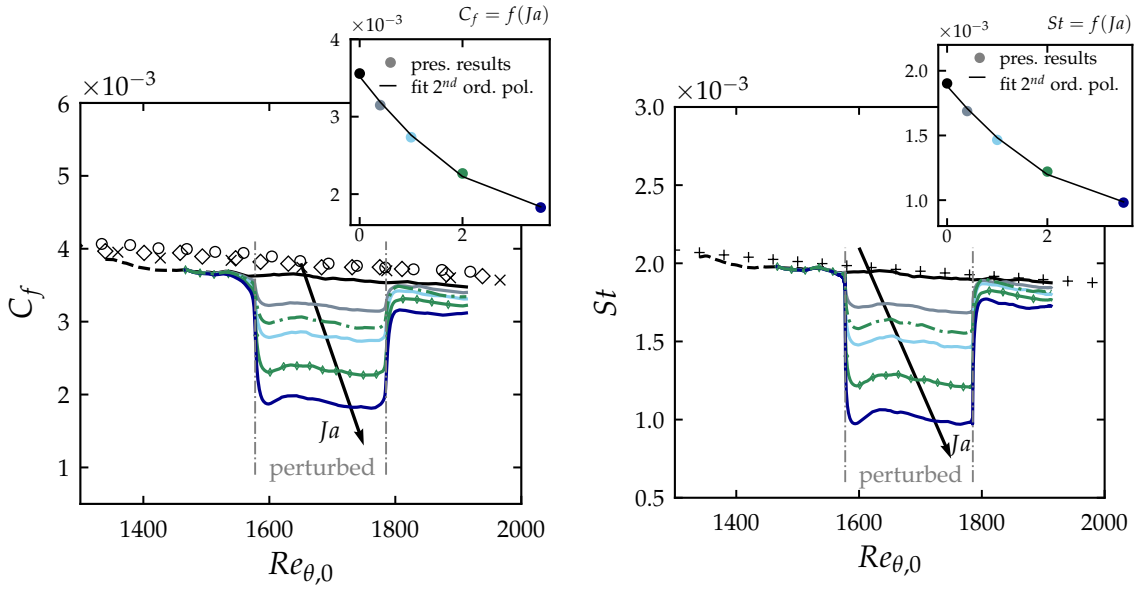

Figure 6: Streamwise evolution of (left) friction coefficient C_f and (right) Stanton number St with the momentum thickness Reynolds number without blowing $Re_{\theta,0}$: (- -), the auxiliary simulation and (—) the main simulation for different values of the Jakob number $Ja = [0, 0.4, 1, 2, 3.52]$, as well as for the uniform blowing (-·-). The latter can be compared in terms of blowing intensity to the case $Ja = 2$ (-♦-). (+), turbulent correlations from [16]; numerical simulations in (◇), [33]; (○), [21]; (×), [30]. The perturbed zone where blowing occurs is also indicated on the graph. The inset figure displays the corresponding evolution with the Jakob number at a fixed $Re_{\theta,0} = 1750$. The points can be fitted with a second order polynomial, $0.0001Ja^2 - 0.0008Ja + 0.003$ for the friction coefficient, and $5.7E-05Ja^2 - 0.00045Ja + 0.0018$ for the Stanton number.

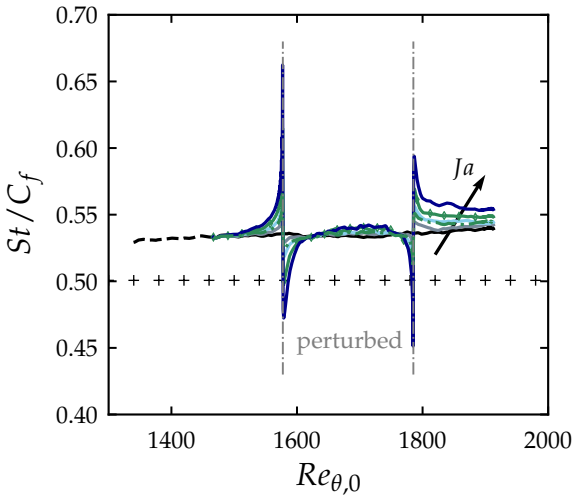

Figure 7: Streamwise evolution of the ratio of the skin-friction coefficient to the Stanton number versus the momentum thickness Reynolds number without blowing $Re_{\theta,0}$: (- -), the auxiliary simulation and (—) the main simulation for different values of the Jakob number $Ja = [0, 0.4, 1, 2, 3.52]$, as well as for the uniform blowing (-·-). The latter can be compared in terms of blowing intensity to the case $Ja = 2$ (-♦-). (+), turbulent correlation from [16].

and the Stanton number St,

$$St = \frac{q_w}{\rho C_p U_\infty \left(\Theta_\infty - \Theta_0\right)}, \tag{15}$$

is depicted in figure 6 as a function of the momentum thickness Reynolds number pertaining the flow without blowing $Re_{\theta,0}$, where $\tau_w = \mu \frac{\partial U}{\partial z}|_{z=0}$ is the mean wall shear stress, $q_w = \lambda \frac{\partial \Theta}{\partial z}|_{z=0}$ is the rate of the heat transfer at the wall to the flow. The present results are compared with data from numerical studies and with the empirical relations from [16] and fairly good agreement is obtained for the case without vaporization, which confirms the validity of the present simulations.

As the incoming boundary layer enters the vaporization region, both C_f and St are significantly reduced. After this initial dip, the curves seem however to be only shifted and to keep the same slope as for the unperturbed flow. Downstream of the blowing region, the values of C_f and St recover the values of the undisturbed flow (i.e. $Ja = 0$) for the lowest Jakob numbers (i.e. $Ja = [0.4, 1]$), indicating that for small blowing rates the flow close to the wall quickly recovers downstream of the perturbed region. For higher Jakob numbers (i.e. $Ja = [2, 3.52]$) this is no longer true and both C_f and St display lower values than the undisturbed flow, suggesting that a high vaporization rate affects the near-wall flow also downstream of the active region. The same trend is observed for the configuration with uniform blowing, with a lower effect on both the friction coefficient and the Stanton number than the corresponding vaporization case at $Ja = 2$. In terms of percentage, it is found that for a fixed $Re_{\theta,0} = 1700$, vaporization diminishes the friction coefficient by 35%, while uniform blowing only by 17%. Similar values are found for the Stanton number.

Figure 7 shows the streamwise evolution of the ratio of the Stanton number St to the friction coefficient Cf versus the momentum thickness Reynolds number, $Re_{\theta,0}$. The ratio St/C_f is around 0.53 for the case without blowing. For both uniform blowing and vaporization, deviations from this value exist, which indicate a loss of the Reynolds analogy. We can observe four peaks in the ratio, occurring upstream and downstream of the two junctions between unperturbed/perturbed flow, around $Re_{\theta,0} \simeq 1590$ and $Re_{\theta,0} \simeq 1790$. Along the perturbed region, where vaporization is active, there seems to be a recovery of the Reynolds analogy between the Stanton number St and the friction coefficient C_f. Ref. [18] explained the presence of these peaks as the result of the mean pressure gradient. In this previous study, blowing is applied through a narrow spanwise slot, which can explain why they authors in [18] observe only two peaks, and a quick recovery towards the Reynolds analogy downstream of the perturbed region. This is not the case in our study, where the ratio is still influenced by the blowing, being higher than the reference value of 0.53. A recovery can be observed but for low vaporization rates. Note finally that uniform blowing has a lower effect than vaporization on the evolution of the ratio St/C_f.

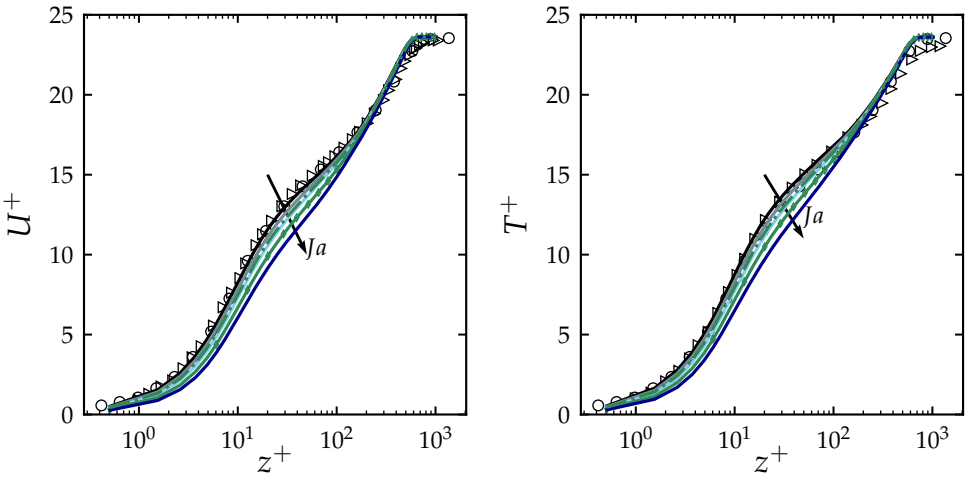

Figure 8: (left) Mean streamwise velocity profile and (right) mean temperature profile, nondimensionalized using the friction velocity from the unperturbed flow $u_{\tau,0}$, as function of the wall distance z^+ for the different values of the Jakob number under investigation and $Re_{\theta,0} = 1684$. (—) evolution for different values of the Jakob number $Ja = [0, 0.4, 1, 2, 3.52]$, as well as for the uniform blowing (-··-). The latter can be compared in terms of blowing intensity to the case $Ja = 2$ (-♦-); the symbols represent literature data for the case of zero velocity at the wall, $Ja = 0$: (◇), DNS data by [33] for $Re_\theta = 1840$ and $Pr = 1$; (○), [21] for $Re_\theta = 1840$.

3.2 Single-point statistics

Next, we examine the effect of blowing on the flow velocity and temperature statistics selected at a fixed downstream location $Re_{\theta,0} = 1684$ (i.e. $x \sim 12\delta_{99,in}$) for different values of the Jakob number. The statistics obtained for a uniform blowing are also considered for comparison. Hereinafter, for all the statistics shown, the non-dimensionalization is done using the local friction velocity of the unperturbed flow $u_{\tau,0}$ at the same position, so that the part of the profiles affected by blowing is easily detected.

Figure 8 shows the mean velocity and temperature profiles as function of the inner wall coordinate z^+. For $Ja = 0$, good agreement is found with the results reported in literature. For non-zero values of the Jakob number, both the linear and the logarithmic layers are modified by the vaporization, with a shift of the profiles downwards. The decrease of the mean velocity and temperature close to the wall is consistent with the decrease of the friction coefficient and Stanton number. At this streamwise location, the blowing affects the velocity and temperature profiles up to $z^+ \sim 200 - 300$, regardless of the vaporization rate Ja. This observation is similar to what found in [19] for the case of a boundary layer subject to uniform blowing.

The difference in the effects generated with vaporization or uniform blowing can also be seen on the mean fields' evolution: a lower effect is observed for uniform blowing on both velocity and temperature mean profiles.

The wall-normal rms profiles of velocity and temperature are shown in figure 9 in inner viscous coordinates for the different values of the Ja under investigation, as well as for the uniform blowing. Literature results are also plotted for validation of the turbulent boundary layer development. Both the streamwise velocity, u^+_{rms}, and temperature fluctuations, θ^+_{rms}, decrease in the presence of vaporization close to the wall while increase in the logarithmic layer. In the outer layer, for $z^+ > 200$, the effect of vaporization becomes negligible. The influence of the vaporization rate on the u^+_{rms} in the vicinity of the wall is displayed in the figure inset, showing a second order polynomial evolution with Ja. The spanwise velocity rms, v^+_{rms}, see panel c of figure 9, is affected by the blowing mainly in the logarithmic layer where it increases with the vaporization rate, whereas the wall-normal velocity fluctuations, w^+_{rms}, increases up to $z^+ \sim 200$. In the vicinity of the wall, the dependence of w^+_{rms} on the Jakob number Ja can be best approximated with a third order polynomial (see inset).

The same remarks can be made on the influence of uniform blowing on the velocity and temperature rms, with the difference that uniform blowing has a less pronounced effect compared to vaporization.

The Reynolds shear stress, $\overline{u'w'}^+$, and the streamwise turbulent heat flux, $\overline{w'\theta'}^+$, are shown in

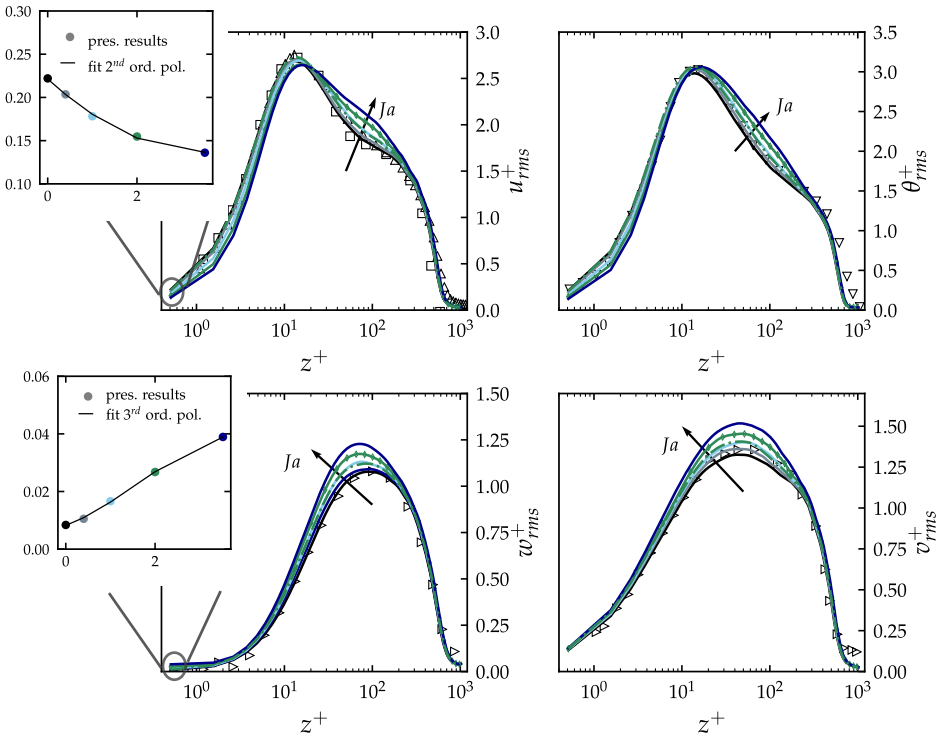

Figure 9: Profiles of the velocity and temperature rms in inner coordinates for the different values of the Jakob number under investigation and $Re_{\theta,0} = 1684$. Uniform blowing is represented by (- - -) and can be compared in terms of blowing intensity to the case $Ja = 2$ (-♦-). In the inset figures, the values at the wall, $z^+ = 0$, of the streamwise and wall-normal rms velocities are plotted versus the Jakob number with the best fitting polynomial: a second order polynomial for the $u^+_{rms}(Ja, Re_{\theta,0} = 1684) = 0.006Ja^2 - 0.047Ja + 0.22$, and a third order polynomial for the $w^+_{rms}(Ja, Re_{\theta,0} = 1684) = -0.0006Ja^3 + 0.003Ja^2 + 0.0055Ja + 0.008$. The symbols report data from the literature for $Ja = 0$: (□), [7] at $Re_\theta = 1000$; (△), [12] at $Re_\theta = 1551$; (▽), [33] at $Re_\theta = 1840$ and (▷), [33] at $Re_\theta = 1410$.

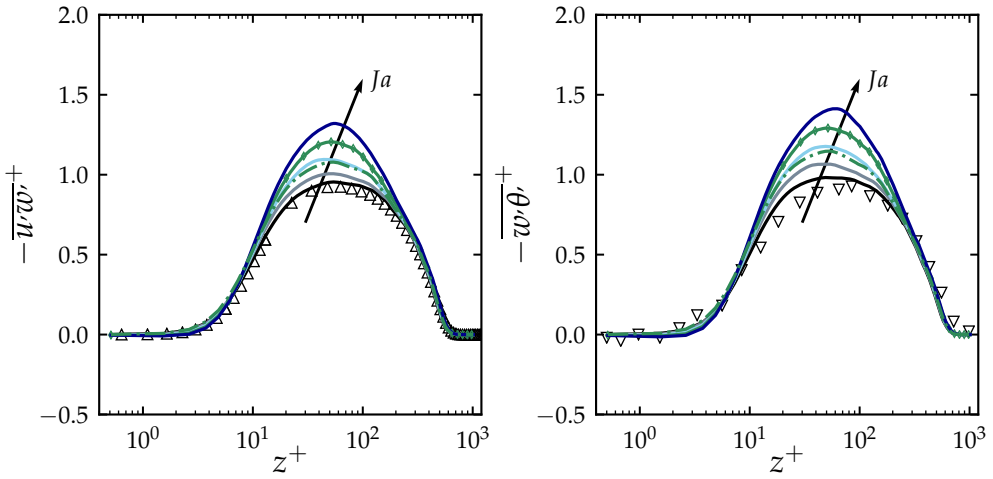

Figure 10: (left) Reynolds shear stress profile and (right) turbulent wall-normal heat flux versus the inner wall coordinate for the different values of the Jakob number under investigation and $Re_{\theta,0} = 1684$. Uniform blowing is represented by (-·-) and can be compared in terms of blowing intensity to the case $Ja = 2$ (-♦-). The symbols pertain data in literature used for comparison in the case $Ja = 0$: (△), [12] at $Re_\theta = 1551$; (▽), [33] at $Re_\theta = 1840$ and $Pr = 1$.

figure 10. The values of $\overline{u'w'}^+$ increase when phase change is active, predominantly in the buffer and logarithmic layer, up to $z^+ \sim 300$. The same behavior can be observed for the wall-normal turbulent heat flux, as shown in the right panel of the same figure. Uniform blowing has a similar but lower effect on both the Reynolds shear stress and the streamwise heat flux.

Next, we examine the different terms in the budget of the turbulent kinetic energy, $k^{'} = \overline{u_i' u_i'}/2$,

$$0 = -U\frac{\partial k^{'}}{\partial x} - W\frac{\partial k^{'}}{\partial z} - \overline{u'w'}\frac{\partial U}{\partial z} - \frac{\partial \overline{w'k'}}{\partial z} - \frac{\partial \overline{w'\,(p/\rho)}}{\partial z} + \nu\frac{\partial^2 k^{'}}{\partial z^2} - \epsilon, \tag{16}$$

with the terms on the right hand side representing the advection by the mean flow, the turbulence production $\left(-\overline{u'w'}\partial U/\partial z\right)$, the turbulent $\left(\partial\overline{w'k'}/\partial z\right)$, viscous $\nu\left(\partial^2 k'/\partial z^2\right)$ and pressure $\left(\frac{\partial\overline{w'(p/\rho)}}{\partial z}\right)$ diffusion and finally the dissipation ϵ. These terms are depicted in figure 11 together with the profiles extracted from the DNS of Li *et al.* [21] at $Re_\theta = 1840$ and Jimenez *et al.* [12] for $Re_\theta = 1100$ presented here for validating the configuration with $Ja = 0$. Indeed, the different datasets agree rather well throughout the entire boundary layer.

The data indicate that the production of kinetic energy shifts away from the wall when the spatio-temporal blowing is active; in the vicinity of the wall the vaporization decreases the production while it increases in the buffer and logarithmic regions. In the case of uniform blowing, it would seem that there is non-significant influence in the viscous sublayer, while the production increases in the buffer and log regions, but less than with vaporization. These results are consistent with the observations made from the analysis of the Q criterion isocontours in figure 3.

The dissipation, on the other hand, decreases in the vicinity of the wall for $z^+ < 3$. This can be explained by the blowing velocity injecting energy into the turbulence and leading to non-vanishing fluctuations closer to the wall. Uniform blowing has very little influence on the dissipation of energy close to wall. Further away, for $z^+ > 3$, the dissipation is slightly increased by both uniform blowing and vaporization.

The advection is increased by blowing, with a higher influence from vaporization than uniform blowing. In the case of a spatially developing boundary layer on a flat plate, the advection is negligible while in the vaporization induced blowing case it presents a minimum of -0.071 around $z^+ \sim 4$ before decreasing away from the wall, for $z^+ > 15$. The diffusion, turbulent, viscous and pressure terms are also altered by blowing. The pressure diffusion is slightly higher near the wall when vaporization happens, while uniform blowing has little effect. The turbulent diffusion is, as the production, shifted from the wall due to the vaporization induced blowing velocity. Additionally, the peak located in the buffer layer increases, showing an enhancement of the turbulent diffusion in this region. Uniform blowing increases the turbulent diffusion, without shifting its profile. Its influence can be observed for $z^+ < 10$, while vaporization has effect until further away from the wall. Finally, very close to the wall, the vaporization induced blowing velocity decreases the viscous

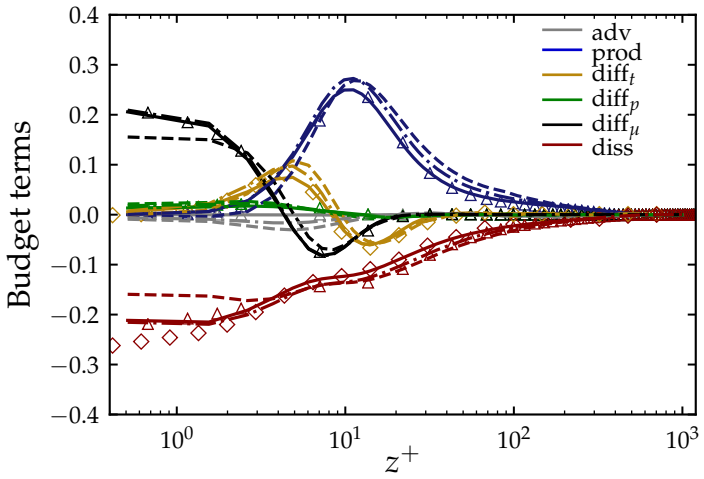

Figure 11: Budget of the turbulent kinetic energy $\overline{u_i' u_i'}/2$ versus the inner wall coordinate z^+ at fixed position, $Re_{\theta,0} = 1684$. Solid lines indicate the flow without blowing $Ja = 0$, dashed lines $Ja = 2$ and dash-dotted lines uniform blowing at $w_b = 0.115\% U_\infty$; the symbols report data from the literature: ($\triangle$), [12] at $Re_\theta = 1100$; ($\diamond$), [21] for $Re_\theta = 1840$. Each term is normalized by $u_{\tau,0}^4/\nu$.

diffusion, while an increase can be observed further away in the buffer layer. Uniform blowing has negligible effect on the viscous diffusion.

This analysis is in agreement with the observations made on the turbulent statistics and the picture provided by the isocontours of the Q-criterion: the vaporization induced blowing velocity injects energy into the flow allowing for non-vanishing eddies closer to the wall, while the dissipation decreases in this region. Further away, in the buffer layer, the advection and diffusion terms increases with the Jakob number and the production is enhanced in the logarithmic layer. Additionally, it can be seen that the turbulent profiles are shifted from the wall, which is in agreement with the findings of [24] who also show that the vortical structures are shifted away from the wall. Uniform blowing has very little influence in the viscous sublayer, while further in the buffer and log layers, its effects are lower than with vaporization.

A transport equation for the temperature variance $k_\theta = \overline{\theta'\theta'}/2$ can be obtained as follows, see among others [32]

$$0 = -W\frac{\partial k_\theta}{\partial z} + \left(-\overline{w'\theta'}\frac{\partial \Theta}{\partial z}\right) - \left(\frac{\partial \overline{w' k_\theta}}{\partial z}\right) + \frac{1}{Pr}\frac{\partial^2 k_\theta}{\partial z^2} - \bar{\epsilon_\theta}, \tag{17}$$

with the first term representing the advection by the mean flow, $\left(-\overline{w'\theta'}\frac{\partial \Theta}{\partial z}\right)$ the production, $\left(-\frac{\partial \overline{w' k_\theta}}{\partial z}\right)$ the turbulent diffusion, $\frac{1}{Pr}\frac{\partial^2 k_\theta}{\partial z^2}$ molecular diffusion and $\bar{\epsilon_\theta}$ dissipation.

The influence of the vaporization on the temperature variance balance equation is similar to that discussed above on the turbulent kinetic energy budget, showing one more time the similarity between velocity and temperature. The production is slightly increased and shifted away from the wall; it is lower for $z^+ < 10$ and higher for $z^+ > 10$. This is due to the increase in the turbulent wall-normal heat flux displayed in figure 10. Away from the wall, $z^+ > 35$, the production balances the dissipation. When vaporization is active, the viscous diffusion decreases in the vicinity of the wall, $z^+ < 2$ while it increases in the buffer layer, $3 < z^+ < 10$. A similar behavior is found for the turbulent diffusion of the temperature variance, which increases close to the wall and reduces in the buffer layer. The dissipation of the temperature variance decreases in the viscous layer and increases further away from the wall, in the logarithmic layer.

The comparison with uniform blowing gives the same observations as for the turbulent kinetic energy. Uniform blowing has negligible influence close to the wall, while further in the buffer and log layers, its influence on the production, diffusion and advection is less important than with vaporization. Dissipation is affected in an equal manner by both vaporization and uniform blowing, for $z^+ > 3.5$, while viscous diffusion is not significantly influenced by uniform blowing.

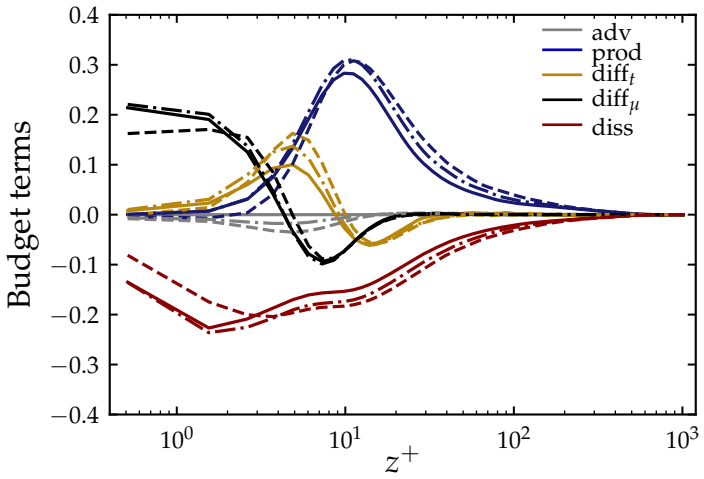

Figure 12: Budget of the temperature variance $\overline{\theta'\theta'}/2$ versus the inner wall coordinate z^+ at a fixed physical position $Re_{\theta,0} = 1684$. Solid lines: flow without blowing $Ja = 0$; dashed lines $Ja = 2$; dash-dotted lines uniform blowing at $w_b = 0.115\%U_\infty$. Each term is normalized by $u_{\tau,0}^2\theta_{\tau,0}^2/\nu$.

3.3 Spectral analysis

The analysis of the turbulent statistics and of the budgets showed that the turbulent structures in the boundary layer are affected by the vaporization. To better quantify these effects, we now resort to a spectral analysis. Note that also for the results presented in this section the non-dimensionalization in wall units is based on the friction velocity of the unperturbed case, $u_{\tau,0}$.

In figure 13 we show isocontours of the pre-multiplied power spectrum of the streamwise velocity component, $k_y\Phi_{uu}$ in inner units, (z^+, λ_y^+), at one streamwise position in the perturbed region for $Ja = 0$ (no blowing), $Ja = 2$ and uniform blowing at constant velocity $w_b = 0.115\%U_\infty$. Note that Φ_{uu} is computed as the Fourier transform of the normalized two point correlation $R_{uu}(x, r, z)$, and that the spanwise wavelength is calculated as $\lambda_y = 2\pi/k_y$, with k_y the spanwise wavenumber. For a better analysis, we also display the isocontours of the difference between perturbed cases, $w_b = 0.115\%U_\infty$ or $Ja = 2$, and the configuration $Ja = 0$. The location and value of the peaks of energy are also displayed in the figures.

At the selected streamwise location, the energy injected during blowing slightly changes the value of the energy peak. We observe an increase from 3.12 to 3.17 for vaporization and a small decrease from 3.12 to 3.07 for uniform blowing, compared to no blowing. The maximum of energy is shifted towards higher wavelengths, from $\lambda_y^+ = 86$ to $\lambda_y^+ = 127$ for uniform blowing, and to $\lambda_y^+ = 113$ for vaporization, and it happens at approximately the same location in the boundary layer, $z^+ = 14$ for both uniform and vaporization induced blowing. Vaporization decreases the energy close to the wall, for $z^+ < 10$ and $\lambda_y^+ > 40$, and it increases it further away, in the buffer and log layers. Uniform blowing has similar effect, but at a lower intensity. In addition, vaporization increases the energy of eddies of all sizes while uniform blowing concentrates on medium to high wavelengths.

The observations above differ from the findings from the spectral analysis conducted by Kametani *et al.* [15], who show how uniform blowing increases the small, short wavelength structures near the wall with more pronounced effects in the outer layer. The differences with our results can be attributed to the non-dimensionalization of the fields. In the present work the friction velocity from the unperturbed flow is used whereas in [15] the local friction velocity is employed, which leads to a biased reading of the results as u_τ is decreased by blowing.

Absolute values of the pre-multiplied cross power spectrum of the streamwise u and wall-normal w velocities, $k_y\Phi_{uw}$, related to the Reynolds shear stress, are reported in figure 14. The energy is increased by both uniform and vaporization-induced blowing. For vaporization, the peak of energy is increased and shifted towards smaller wavelengths and closer to the wall. Uniform blowing changes little the peak's location, while its increase is less important than with vaporization. Both uniform blowing and vaporization induce energy at smaller wavelengths, mainly in the buffer and log layers. This extra energy is present on a larger wall-normal region for vaporization than for the flow with uniform blowing. A distinctive second peak can be observed in the energy spectra generated by vaporization, located at $(250, 80)$. This shows that large wavelengths, i.e. large eddies, are enhanced in the log layer.

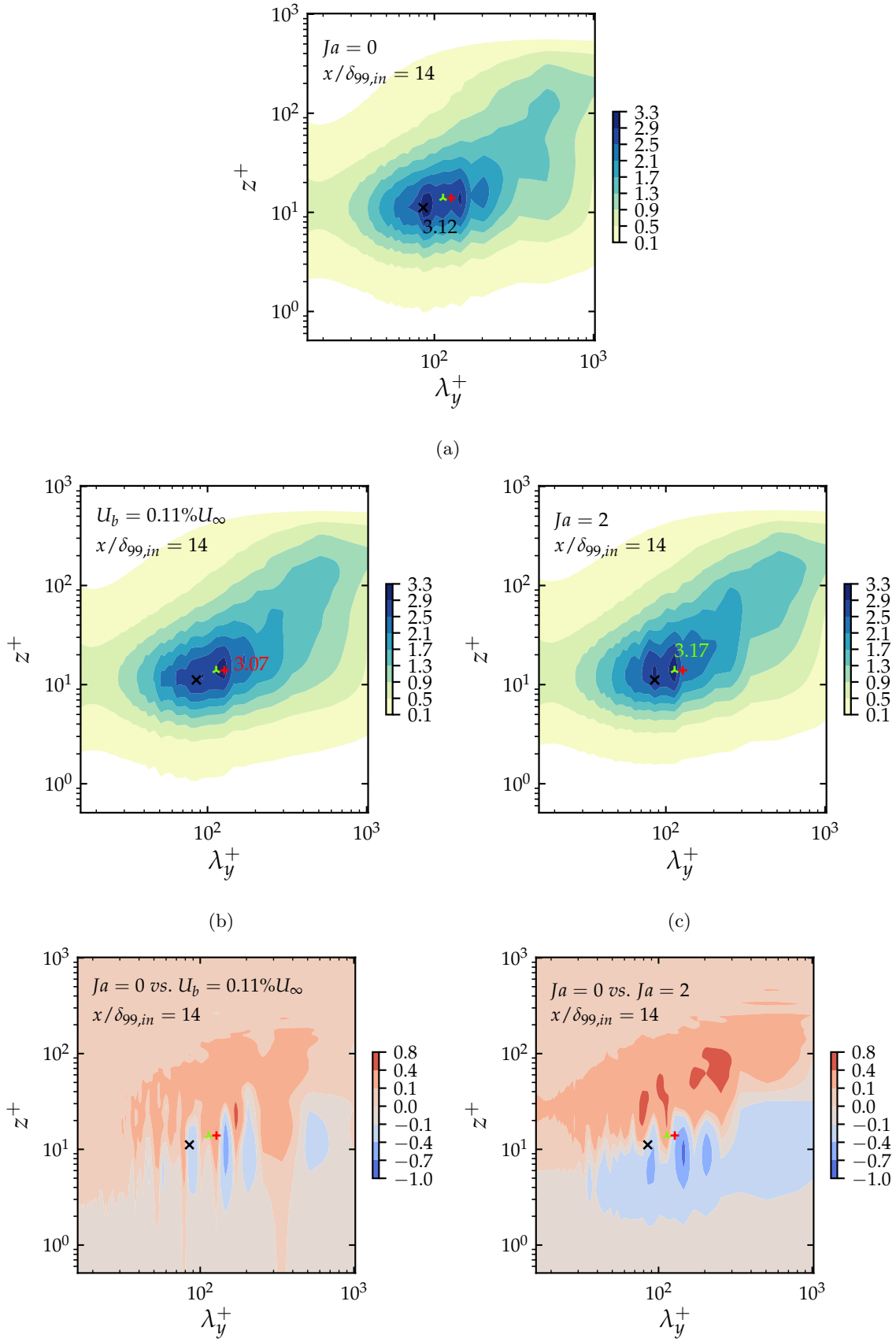

Figure 13: (a)-(c) Isocontours of the pre-multiplied power spectrum of the streamwise velocity, $k_y\Phi_{uu}/u_{\tau,0}^2$, plotted on inner-scaled axes at $x/\delta_{99,in} = 14$. (a) Flow without phase change ($Ja = 0$), (b) with uniform blowing, $w_b = 0.115\%U_\infty$ and (c) with vaporization induced blowing, $Ja = 2$. The peaks of energy and their locations are indicated by symbols: (x) for $Ja = 0$, (+) for $w_b = 0.115\%U_\infty$, and (人) for $Ja = 2$. (d)-(e) isocontours of the difference between the perturbed case ($w_b = 0.115\%U_\infty$ (d) and $Ja = 2$ (e)) and the configuration $Ja = 0$.

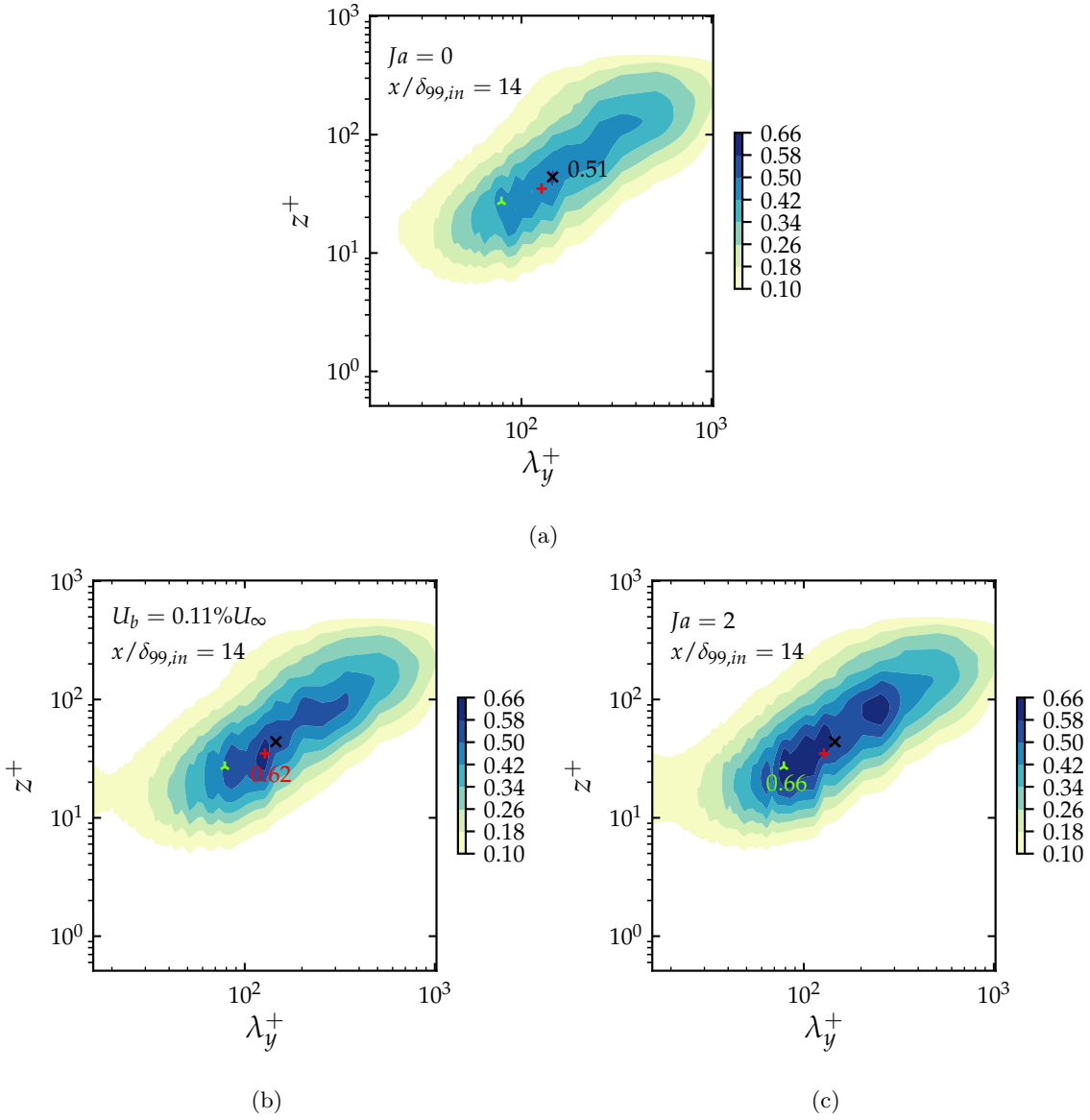

Figure 14: Isocontours of the pre-multiplied cross power spectrum of the streamwise and wall-normal velocities, $-\left(k_y \Phi_{uw}/u_{\tau,0}^2\right)$, plotted on inner-scaled axes at $x/\delta_{99,in} = 10$. (a) Flow without phase change ($Ja = 0$), (b with uniform blowing, $w_b = 0.115\%U_\infty$ and (c) with vaporization induced blowing, $Ja = 2$. The peaks of energy and their locations are indicated by symbols: (**x**) for $Ja = 0$, (+) for $w_b = 0.115\%U_\infty$, and (人) for $Ja = 2$.

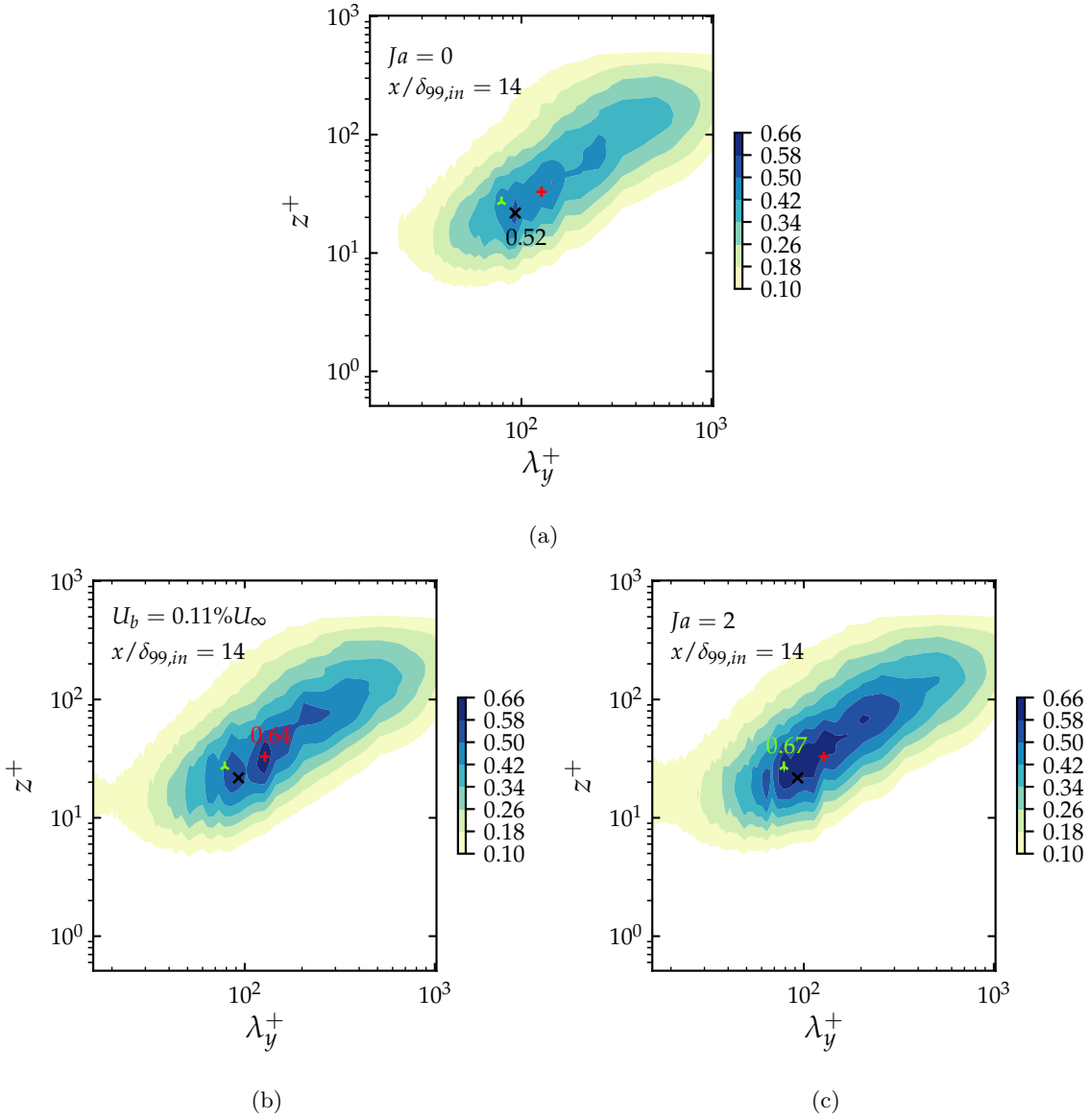

Figure 15: Isocontours of the pre-multiplied cross power spectrum of the wall-normal velocity and temperature, $-(k_y \Phi_{w\theta}/(u_{\tau,0}\theta_{\tau,0}))$, plotted on inner-scaled axes at $x/\delta_{99,in} = 10$. (a) Flow without phase change ($Ja = 0$),(b) with uniform blowing $w_b = 0.115\%U_\infty$, and (c) with vaporization induced blowing, $Ja = 2$. The peaks of energy and their locations are indicated by symbols: ($\mathbf{x}$) for $Ja = 0$, ($+$) for $w_b = 0.115\%U_\infty$, and (人) for $Ja = 2$.

To conclude, figure 15 displays isocontours of the pre-multiplied cross power of the wall-normal heat flux, in absolute value, i.e. $-\left(k_y \Phi_{w\theta} / \left(u_{\tau,0}\theta_{\tau,0}\right)\right)$. The vaporisation highly increases the spectrum energy of the normal heat flux. The range of wavelength and wall distance of the spectra is spread by both uniform blowing and vaporization. The peak of energy is slightly increased in both cases. However, uniform blowing shifts it towards larger wavelengths and further away from the wall while vaporization creates a maximum of energy at smaller wavelengths. In both cases, energy is forced at very small wavelengths in the buffer layer, on a larger wall-normal layer in the flow affected by vaporization. A small second peak of energy emerges for large wavelengths and further away of the wall, at $(250, 70)$. Given the similarity velocity-temperature, these results are consistent with what is observed in the case of the pre-multiplied cross power of the shear stress, $k_y \Phi_{uw}$.

4 Conclusions

In the present work, we report data from DNS of the spatial boundary layer flow developing inside the gas phase, a superheated vapor, over an evaporating liquid film at saturation temperature whose surface is assumed flat and of constant height. Here, the vaporization of the static liquid pool is represented by a boundary condition on the normal velocity component of the vapour flow. This non-zero normal velocity induced by vaporization is computed at each time step using the thermal gradient at the interface. The temperature and momentum equations are therefore coupled via the convective term in the vapor phase in the energy equation and the boundary conditions for the fluid velocity.

The analysis of the effects of this unsteady and non-uniform blowing at the wall on the structure of the boundary layer flow, has lead to a series of observations. The momentum boundary layer thickness increases with the vaporization rate. The influence of the blowing on the mean profiles is visible predominantly in the inner region, where a decrease can be observed when increasing the Jakob number, i.e. the blowing speed associated to a given temperature gradient. Both the friction coefficient and the Stanton number are therefore significantly reduced in the vaporization region. Downstream of this region, for low vaporization rate, the curves recover the evolution observed without blowing, while for higher rates, the curves are shifted.

These results are similar to what was previously observed for uniform blowing. To highlight the differences obtained with vaporization, simulations with a constant blowing velocity have been conducted. It has been found that the effect of uniform blowing on the global measures examined here, mean and rms fields, is less important than in the flow with vaporization, for the same mean intensity of blowing. As concerns the wall friction and Stanton number, it is found that the vaporization induced decrease is twice that with uniform blowing.

The analysis of the turbulent kinetic energy budget also reveals particularly rich dynamics. The production is shifted away from the wall; close to the wall the vaporization decreases the production while further away in the buffer and logarithmic layers there is an increase of energy production. Close to the wall the vaporization induced energy decreases the dissipation rate by allowing the existence of non-vanishing eddies closer to the wall. The diffusion terms are also modified by vaporization, decreased in the vicinity of the wall and increased in the buffer layer, with little influence in the logarithmic layer. Similar influence of the vaporization on the temperature variance balance equation is found, confirming one more time the similarity between velocity and temperature. Uniform blowing influences very little the budgets in the viscous sublayer. Both viscous and pressure diffusion are almost unchanged while the increase in the turbulent diffusion is less pronounced than in the case with vaporization.

Spectral analysis of the streamwise velocity fluctuations, Reynolds shear stress and the wall-normal turbulent heat flux have also been conducted. The isocontours of the power spectra of the streamwise velocity show that, at the selected streamwise location, the energy injected during vaporization decreases the spectrum content close to the wall and increases it in the buffer and log layers. This can be seen as a shift of energy further away from the wall. Uniform blowing has similar but lower effect. Additionally, it does not affect the structures of all sizes, as it is the case for vaporization. The analysis of the pre-multiplied cross power spectrum of the streamwise and wall-normal velocities reveals that the energy injected by vaporization highly increases the energy of the shear stress, with a maximum value shifted closer to the wall and happening for smaller scales. Additionally, a second peak of energy emerges, showing that large wavelengths, i.e. large eddies, are enhanced in the log layer. Uniform blowing induces a similar increase, however of a lower amplitude. In addition, the location of the peak of the energy is close to that with no perturbation and no distinct second peak can be observed. Finally, the analysis of the energy spectrum of the

turbulent heat flux in the wall-normal direction indicates an increase of energy in the logarithmic layer. The peak of energy is slightly increased for both types of perturbation. However, uniform blowing shifts the energy peak towards larger wavelengths and further away from the wall while vaporization induces a maximum of energy at smaller wavelengths.

The analysis conducted here does not consider deformation of the liquid interface and it is valid in the limit of high-density ratio and low pressure environments. Recent studies have indeed shown that surface tension might alter the near wall dynamics in turbulence [28]. Therefore, in a near future, we plan to consider also the presence of the liquid layer at wall by simulating its dynamics and the induced evaporation, see e.g. Scapin *et al.* [29].

Acknowledgements

The authors gratefully acknowledge the CNES (Centre National d'tudes Spatiales) and Air Liquid Advanced Technologies for the financial support. The authors acknowledge access to the HPC resources of CINES under the allocation A0072B10285 by GENCI in France, as well as to the resources provided by UNINETT Sigma2 the National Infrastructure for High Performance Computing and Data Storage in Norway, project number NN9561K.

Declaration of Interests

The authors report no conflict of interest.

References

[1] G. Araya, S. Leonardi, and L. Castillo. "Passive scalar statistics in a turbulent channel with local time-periodic blowing/suction at walls". In: *Physica D* 237.14-17 (2008), pp. 2190–2194.

[2] G. Araya, S. Leonardi, and L. Castillo. "Steady and time-periodic blowing/suction perturbations in a turbulent channel flow". In: *Physica D* 240.1 (2011), pp. 59–77.

[3] H. Choi, P. Moin, and J. Kim. "Active turbulence control for drag reduction in wall-bounded flows". In: *J. Fluid Mech.* 262 (1994), pp. 75–110.

[4] P. Costa. "A FFT-based finite-difference solver for massively-parallel direct numerical simulations of turbulent flows". In: *Comput. Math. with Appl.* 76.8 (2018), pp. 1853–1862.

[5] G. Desoutter et al. "DNS and modeling of the turbulent boundary layer over an evaporating liquid film". In: *Int. J. Heat Fluid Flow* 52.25-26 (2009), pp. 6028–6041.

[6] G. Hasanuzzaman et al. "Experimental investigation of turbulent boundary layers at high Reynolds number with uniform blowing, part I: statistics". In: *J. Turbul.* 21.3 (2020), pp. 129–165.

[7] H. Hattori, T. Houra, and Y. Nagano. "Direct numerical simulation of stable and unstable turbulent thermal boundary layers". In: *Int. J. Heat Fluid Flow* 28.6 (2007), pp. 1262–1271.

[8] J. C. R. Hunt, A. A. Wray, and R. Moin. "Eddies, streams, and convergence zones in turbulent flows". In: *CTR Research Briefs* (1988).

[9] Y. Iritani, N. Kasagi, and M. Hirata. "Heat transfer mechanism and associated turbulence structure in the near-wall region of a turbulent boundary layer". In: *Turb. Shear Flows 4.* 1985, pp. 223–234.

[10] N. Jarrin et al. "A synthetic-eddy-method for generating inflow conditions for large-eddy simulations". In: *Int. J. Heat Fluid Flow* 27.4 (2006), pp. 585–593.

[11] J. Jimenez et al. "Turbulent shear flow over active and passive porous surfaces". In: *J. Fluid Mech.* 442 (2001), p. 89.

[12] J. Jiménez et al. "Turbulent boundary layers and channels at moderate Reynolds numbers." In: *J. Fluid Mech.* 657 (2010), pp. 335–360.

[13] Y. Kametani and K. Fukagata. "Direct numerical simulation of spatially developing turbulent boundary layer for skin friction drag reduction by wall surface-heating or cooling". In: *J. Turbul* 13 (2012), N34.

[14] Y. Kametani and K. Fukagata. "Direct numerical simulation of spatially developing turbulent boundary layers with uniform blowing or suction". In: *J. Fluid Mech.* 681 (2011), pp. 154–172.

[15] Y. Kametani et al. "Effect of uniform blowing/suction in a turbulent boundary layer at moderate Reynolds number". In: *Int. J. Heat Fluid Flow* 55 (2015), pp. 132–142.

[16] W.M. Kays and M.E. Crawford. In: *Convective Heat and Mass Transfer*. McGraw-Hill, 1993.

[17] J. Kim, K. Kim, and H. J. Sung. "Wall pressure fluctuations in a turbulent boundary layer after blowing or suction". In: *AIAA journal* 41.9 (2003), pp. 1697–1704.

[18] H. Kong, H. Choi, and J. S. Lee. "Dissimilarity between the velocity and temperature fields in a perturbed turbulent thermal boundary layer". In: *Phys. Fluids* 13.5 (2001), pp. 1466–1479.

[19] P.-A. Krogstad and A. Kourakine. "Some effects of localized injection on the turbulence structure in a boundary layer". In: *Phys. Fluids* 12.11 (2000), pp. 2990–2999.

[20] D. Lakehal et al. "Turbulence and heat exchange in condensing vapor-liquid flow". In: *Phys. Fluids* 20.6 (2008), p. 065101.

[21] D. Li, K. Luo, and J. Fan. "Direct numerical simulation of heat transfer in a spatially developing turbulent boundary layer". In: *Phys. Fluids* 28.10 (2016), p. 105104.

[22] M. A. Miller, A. Martin, and S. CC. Bailey. "Investigation of the scaling of roughness and blowing effects on turbulent channel flow". In: *Exp. Fluids.* 55.2 (2014), p. 1675.

[23] G. Oh et al. "Extended synthetic eddy method to generate inflow data for turbulent thermal boundary layer". In: *Int. J. Heat Mass Transfer* 134 (2019), pp. 1261–1267.

[24] J. Park and H. Choi. "Effects of uniform blowing or suction from a spanwise slot on a turbulent boundary layer flow". In: *Phys. Fluids* 11.10 (1999), pp. 3095–3105.

[25] A. E. Perry and P. H. Hoffmann. "An experimental study of turbulent convective heat transfer from a flat plate". In: *J. Fluid Mech.* 77.2 (1976), pp. 355–368.

[26] E.-R. Popescu, S. Tanguy, and C. Colin. "On the influence of liquid/vapor phase change onto the Nusselt number of a laminar superheated or subcooled vapor flow". In: *International Journal of Thermal Sciences* 140 (2019), pp. 397–412.

[27] M. Quadrio, J. M. Floryan, and P. Luchini. "Effect of streamwise-periodic wall transpiration on turbulent friction drag". In: *J. Fluid Mech.* 576.004 (2007), pp. 425–444.

[28] A. Roccon, F. Zonta, and A. Soldati. "Turbulent drag reduction by compliant lubricating layer". In: *J. Fluid Mech.* 863 (2019).

[29] N. Scapin, P. Costa, and L. Brandt. "A volume-of-fluid method for interface-resolved simulations of phase-changing two-fluid flows". In: *J. Comp. Phys.* 407 (2020), p. 109251.

[30] P. Schlatter et al. "Simulations of spatially evolving turbulent boundary layers up to $Re_\theta = 4300$". In: *Int. J. Heat Fluid Flow* 31.3 (2010), pp. 251–261.

[31] A. Singha, Md. A. Al Faruque, and R. Balachandar. "Vortices and large-scale structures in a rough open-channel flow subjected to bed suction and injection". In: *J. Eng. Mech.* 138.5 (2012), pp. 491–501.

[32] Y. Sumitani and N. Kasagi. "Direct numerical simulation of turbulent transport with uniform wall injection and suction". In: *AIAA journal* 33.7 (1995), pp. 1220–1228.

[33] X. Wu and P. Moin. "Transitional and turbulent boundary layer with heat transfer". In: *Phys. Fluids* 22.8 (2010), p. 085105.

[34] S. Yoshioka and P.H. Alfredsson. "CONTROL OF TURBULENT BOUNDARY LAYERS BY UNIFORM-WALL SUCTION AND BLOWING". In: *IUTAM Symp.on Laminar-Turbulent Trans.* 2006, pp. 437–442.